Many-body effects in praesodymium core-level spectroscopies of PrO_2

A. Bianconi
Dipartimento di Fisica, Università degli Studi di Roma "La Sapienza," 00185 Roma, Italy

A. Kotani and K. Okada
Department of Physics, Faculty of Science, Tohoku University, Sendai 980, Japan

R. Giorgi and A. Gargano
Centro Ricerche Energia Alternativa Casaccia, ENEA, S. S. Anguillarese 301, 00100 Roma, Italy

A. Marcelli
Laboratori Nazionali di Frascati–INFN, 00044 Frascati, Italy

T. Miyahara
Photon Factory, National Laboratory for High Energy Physics, Oho-Machi, Tsukuba gun, Ibaraki-ken, 305 Japan
(Received 23 September 1987; revised manuscript received 12 February 1988)

The high-energy deep-core-level spectra of PrO_2 have been studied. Pr $3d$ x-ray photoemission spectroscopy (XPS), Pr $M_{4,5}$ x-ray-absorption spectroscopy (XAS) and Pr L_3 XAS show many-body effects. The data are analyzed in the framework of the filled-band Anderson-impurity model. Starting from the many-body description of the ground-state, the final states of each core-level spectroscopy are predicted. The effective relaxation energy in the final state decreases going from $3d$ XPS to L_3 XAS to $M_{4,5}$ XAS because of the repulsive interaction between the excited electron and the $4f$ electron in XAS spectra. It is shown that the ground state exhibits mixing of many-body configurations $4f^1$ and $4f^2\underline{L}$, where $\underline{L}$ denotes a hole in the oxygen $2p$-derived valence band, separated by the energy $\Delta E = 0.5$ eV. A nonzero probability of the occupation of the $4f^2\underline{L}$ configuration, giving a noninteger $4f$ count $n_f = 1.6$, is found.

INTRODUCTION

The particular case in solid-state physics of cerium dioxide (CeO_2) has been the object of much interest in these last ten years[1–15] because in this crystal the one-electron approximation breaks down for large electronic correlation, and the quantum-mechanics effect of the multielectron configuration interaction plays a key role in the description of its properties. PrO_2 has a similar crystal CaF_2 structure but it is black and conducting[16] while CeO_2 is transparent and insulating.

In the framework of a one-electron description both CeO_2 and PrO_2 exhibit a similar electronic structure.[3] They have a filled oxygen $2p$ band and because the metal atoms contribute to the filling of this band with their four electrons they can be considered in principle "tetravalent" compounds. But it has been shown that in these compounds there is a breakdown of the band density for an f partial wave both at the metal and the oxygen sites; in other words there is strong covalent bonding and therefore f states occur both in the oxygen $2p$ band, which gives delocalized band behavior, and above the valence band, which is more localized and does not contribute to the bonding.

The presence of strong covalent bonding involving f electrons cannot be explained in an uncoupled scheme in which there are only two configurations $4f^0$ ($4f^1$) and $4f^1$ ($4f^2$) well separated in energy without hybridization in CeO_2 (PrO_2).

The ground state of CeO_2 should be described by a mixing of two electronic configurations $4f^0$ and $4f^1\underline{L}$, where $\underline{L}$ indicates a hole in the oxygen (ligand) $2p$ valence band, according to the cluster model of Fujimori[4] and the filled-band Anderson-impurity model.[6–12] For cerium metallic compounds the theoretical results for the Anderson-impurity Hamiltonian have led to a unified interpretation of much of the high-energy-scale spectroscopic and low-energy-scale transport data.[17–21] Recently it has been proposed that CeO_2 is a prototype of a class of correlated covalent systems called interatomic intermediate-valence (IIV) systems which are described by mixing between $4f^n$ and $4f^{n+1}\underline{L}$ configurations separated by the energy ΔE, and where the hybridization energy V is of the same order of magnitude as ΔE.[11]

Here we have studied the formally tetravalent rare-earth compound PrO_2 with several core spectroscopies in order to probe the ground state by different final states. We have measured the Pr $3d$ x-ray photoemission spectra (XPS) and the $\underline{L}_3$-edge x-ray-absorption spectra (XAS). All spectra show many-body effects.

Starting from the description of the ground state in terms of mixing between the $[4f^1]$ and $[4f^2\underline{L}]$ configurations separated by energy ΔE it is possible to interpret the different core-level spectroscopies by the filled-band Anderson-impurity model. The final states are different in each spectrum. The $3d$ XPS shows the satellites $\underline{3d}4f^2\underline{L}$ and $\underline{3d}4f^3\underline{L}^2$ at lower binding energy than the $\underline{3d}4f^1$ main line. The L_3 XAS spectrum shows

splitting of the white line at threshold due to excitation of the photoelectron to the unoccupied $5,\varepsilon d$ states, at the Pr atomic site, at energy $\varepsilon_d(k)$, derived from $5d$ atomic orbitals.[10] It is shown that the two main peaks observed in the PrO_2 L_3 XAS are mainly due to $\underline{2p}[4f^1]5,\varepsilon d$ and $\underline{2p}[4f^2\underline{L}]5,\varepsilon d$ final states. Finally using the same theoretical approach the final states in the $3d$ x-ray-absorption spectra have been calculated and compared with the experimental spectrum measured by Karnatak *et al.*[15]

In the final states the effective perturbation energy in core-level spectroscopy is $-U_{fc}$ (the Coulomb attraction between the core c and f electrons) in XPS; $-U_{fc}+U_{fd}$ (where U_{fd} is the Coulomb repulsion between the f and the excited $5d$ electron) in L_3 XAS; and $-U_{fc}+U_{ff}$ in $M_{4,5}$ XAS. Therefore the final-state perturbation decreases going from XPS to L_3 XAS and to $M_{4,5}$ XAS spectra.

EXPERIMENT

XPS spectra were recorded by using a hemispherical electron analyzer and the aluminum $K\alpha$ x-ray-emission line. The total instrumental energy resolution was 1.5 eV.

The samples were stoichiometric PrO_2 and CeO_2 polycrystalline powder prepared by L. Albert and P. E. Caro at the Laboratoire d'Elements de Transition dans les Solides at Meudon (France). The samples were pressed on indium metal and introduced in the experimental chamber without breaking the vacuum from a preparation chamber. The electron-energy distribution curves were recorded rapidly after introducing the samples. The $3d$ XPS spectra were obtained by summing 80 scans to get a good signal-to-noise ratio and no variation of the spectra was observed during exposure to the x-ray beam. The Auger and XPS spectra over a wide range do not show the presence of either carbon contamination or other atomic impurities on the surface. The $3d$ XPS experiment of PrO_2 was repeated at the Photon Factory synchrotron radiation facility in Tsukuba using x-ray photon energy tuned between 2000 and 3000 eV in order to decrease the surface sensitivity and to exclude the contribution of reduced atoms on the surface. No variation of the Pr $3d$ XPS spectrum has been found by increasing bulk sensitivity, therefore the spectrum can be associated with bulk properties of PrO_2.

The L_3 absorption spectra were measured at the Adone storage ring of the Frascati synchrotron radiation facility using a Si(220) channel-cut crystal and by operating with the storage ring at 1.2 GeV to suppress high-harmonics contamination of the monochromatized beam.

RESULTS

Figure 1 shows the Pr $3d$ XPS spectrum of PrO_2. The binding energy is measured from the top of the valence band. The XPS spectrum shows a shoulder in the high-energy tail beyond 970 eV which is due to the tail of the oxygen $1s$ Auger line that can be subtracted from the spectrum of direct photoemission excitations. We observe a spin-orbit-splitting energy $\Delta_{s.o.}$ of 20.6 eV between the Pr $3d_{5/2}$ and Pr $3d_{3/2}$ lines. Each core-level spectrum shows the features A, B, and C separated by $\Delta_{s.o.}$. The peak A of the $3d_{5/2}$ spectrum is partially overlapped by the peak C of the $3d_{3/2}$ spectrum. The intensity ratio between the two spin-orbit components is in agreement with the expected statistical ratio of $\frac{2}{3}$. Using

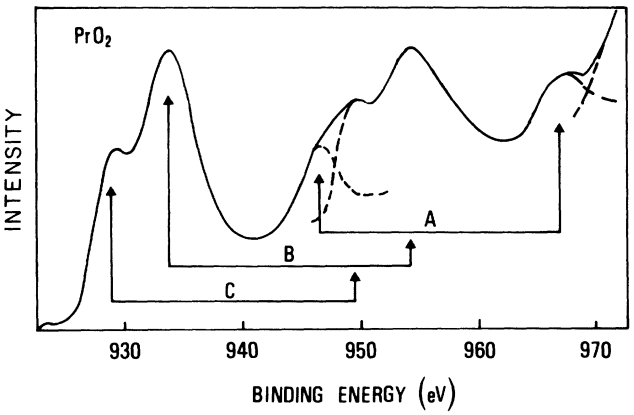

FIG. 1. XPS spectrum of Pr $3d$ core level of PrO_2. The three components A, B, and C of the $3d$ core spectrum ($M_{4,5}$) are split into $3d_{5/2}$ and $3d_{3/2}$ components by spin-orbit energy 20.6 eV.

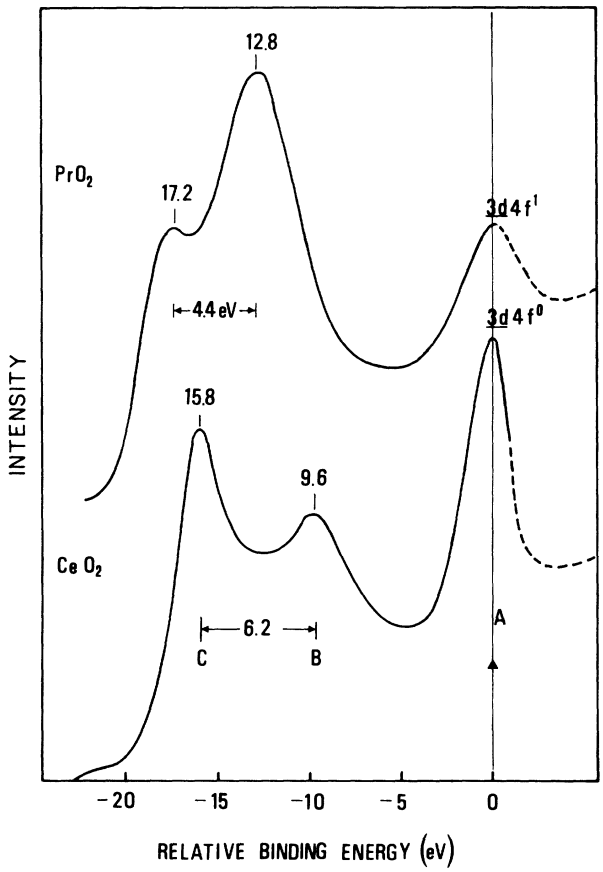

FIG. 2. XPS spectrum of Pr $3d_{5/2}$ core level of PrO_2 compared with the Ce $3d_{5/2}$ XPS spectrum of CeO_2. The spin-orbit components $3d_{5/2}$ and $3d_{3/2}$ have been separated by a similar procedure.

this intensity ratio and the spin-orbit splitting of 20.6 eV the $3d_{5/2}$ spectrum has been separated from the $3d_{3/2}$ spectrum as shown in Fig. 2.

Figure 2 reports the comparison between the $3d$ core-level XPS spectra of CeO_2 and PrO_2. The spectrum of the Ce $3d_{5/2}$ core level was obtained with the same method, and it is in agreement with previous results.[6]

The spectra have been aligned to the peaks A and the energy of peak A is taken as zero of the energy scale. The two spectra show similar series of satellites following the excitation of the $3d$ core hole. Important differences concern the intensity ratio of peaks B and C which is reversed and their energy splitting which is 6.2 eV in CeO_2 and 4.4 eV in PrO_2. Moreover the energy separation between peaks A and C increases from 15.8 to 17.2 eV going from CeO_2 to PrO_2. In analogy with the CeO_2 spectrum we assign the peaks A, B, and C in the PrO_2 XPS to the $\underline{3d}4f^1$, $\underline{3d}4f^2\underline{L}$, and $\underline{3d}4f^3\underline{L}^2$ final-state configurations, whereas the latter two configurations are mixed with each other considerably.

In Fig. 3 the $3d_{5/2}$ XPS spectrum of PrO_2 is compared with the $3d_{5/2}$ XAS spectrum measured by Karnatak *et al.*[15] In the $3d_{5/2}$ XAS final states the white lines are due to dipole transition where one core Pr $3d$ electron is promoted into a Pr $4f$ state giving the excited states of the N-electron system because the number of electrons is the same in the initial and final states. In this figure the same energy scale indicates the binding energy, referred to the Fermi level, of core levels for the XPS spectrum. The energy of the XPS lines gives the energy of the excited configurations of the $(N-1)$-electron system; in fact, in the XPS experiment one electron, emitted in the vacuum, is missing.

The XAS final-state configurations $3d4f^2$ and $3d4f^3\underline{L}$ which give origin to the white line and its satellite are determined by core transitions from ground state $\Psi_g = |4f^1\rangle + b\,|4f^2\underline{L}\rangle$ where one $3d$ core electron is moved from the $3d$ core level into the $4f$ level. The

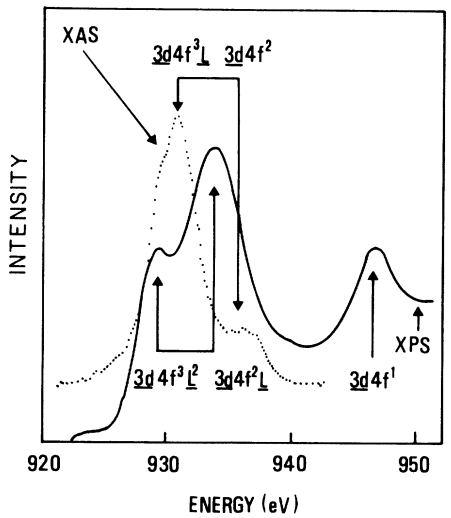

FIG. 3. Comparison between the $3d$ XAS absorption spectrum measured by Karnatak *et al.* (Ref. 15) (dotted line) and the $3d_{5/2}$ XPS spectrum (solid line) of PrO_2.

$\underline{3d}4f^2$ and $3d4f^3\underline{L}$ final-state configurations are close in energy and therefore are strongly mixed by the mixing energy.

The energy separation between the *ionic* final states in XPS and XAS which are only different for one $\underline{L}$ hole give the energy required for the excitation of the ligand hole, which is an important parameter for the description of the ground state. In fact, the difference $E_{XPS}\{\underline{3d}4f^2\underline{L}\}-E_{XAS}\{\underline{3d}4f^2\}$, where the brackets $\{\ \}$ indicate the ionic configurations, gives the energy to add a ligand hole to the $4f^2$ configuration. The energy to add a ligand hole plays an important role in the determination of the energy separation between $4f^1$ and $4f^2\underline{L}$ ionic configurations in the ground state. The observed energy of the spectral features in the XPS and XAS spectra are shifted by the mixing energy and therefore it is necessary to make a theoretical many-body analysis of the spectra to extract the ligand hole excitation energy.

The mixing energy increases the energy separation between the ionic XAS final states $\underline{3d}4f^3\underline{L}$ and $\underline{3d}4f^2$ and changes their intensity ratio in such a way that it is not possible to separate the two configurations giving origin to the main line and the satellite in the XAS spectra of Fig. 3. Only for classification purposes are the two spectral features sometimes indicated by $(\underline{3d}4f^3\underline{L})$ and $(\underline{3d}4f^2)$, respectively.

The energy positions of the peaks in the $3d$ XAS absorption spectrum are found to be very close to the energy positions of peaks B and C in the $3d$ XPS spectrum. The origin of the low-binding-energy XPS peaks is determined by mixing in the final state of the $\underline{3d}4f^2\underline{L}$ ionic configuration and of the shakedown $\underline{3d}4f^3\underline{L}^2$. It is clear that the energy separation between the XPS ionic configuration of the shakedown $\underline{3d}4f^3\underline{L}^2$ and the XAS $\underline{3d}4f^3\underline{L}$ provides the energy to excite a ligand hole in the $4f^3$ configuration.

The energy difference between the average energy of the XAS spectral features and the average energy of peaks B and C in the $3d$ XPS, shown in Fig. 3, is very small, indicating that the energy for ligand hole excitation in PrO_2 is small. In order to extract the f occupation number n_f in the ground state it is necessary to calculate the different final states in the $3d$ XPS, $3d$ XAS, and L_3 XAS by a many-body theory excited from the same ground state.

The theoretical calculations of the Pr $3d$ XPS and $3d$ XAS of PrO_2, made by using the recently developed approach[6-9] in the frame of the Anderson-impurity model with a filled valence band (discussed in the next section), are shown in Fig. 4.

The Pr L_3 absorption spectrum is shown in Fig. 5. The white line is mostly due to a resonance in the atomic part of the total cross section for atomic $2p \rightarrow 5,\varepsilon d$ transitions.[11] The two white lines have been assigned mainly to $\underline{2p}[4f^1]5,\varepsilon d$ and $\underline{2p}[4f^2\underline{L}]5,\varepsilon d$ final states. The many-body calculation for the $2p \rightarrow 5,\varepsilon d$ transition in PrO_2 is reported in the same figure.

THEORETICAL ANALYSIS

The Hamiltonian of our system is written as

$$H=\sum_{k,\nu}\varepsilon_v(k)a_v^\dagger(k,\nu)a_v(k,\nu)+\sum_k\varepsilon_d(k)a_d^\dagger(k)a_d(k)+\varepsilon_f^0\sum_\nu a_f^\dagger(\nu)a_f(\nu)+\varepsilon_c a_c^\dagger a_c$$
$$+\frac{V}{\sqrt{N}}\sum_{k,\nu}[a_v^\dagger(k,\nu)a_f(\nu)+a_f^\dagger(\nu)a_v(k,\nu)]+U_{ff}\sum_{\substack{\nu,\nu'\\(\nu>\nu')}}a_f^\dagger(\nu)a_f(\nu)a_f^\dagger(\nu')a_f(\nu')$$
$$+\frac{U_{fd}}{N}\sum_{k,k',\nu}a_f^\dagger(\nu)a_f(\nu)a_d^\dagger(k)a_d(k')-(1-a_c^\dagger a_c)\left[U_{fc}\sum_\nu a_f^\dagger(\nu)a_f(\nu)+\frac{U_{dc}}{N}\sum_{k,k'}a_d^\dagger(k)a_d(k')\right].$$

Here, $\varepsilon_v(k)$, $\varepsilon_d(k)$, ε_f^0, and ε_c are the energies of the O $2p$ valence band, Pr $5d$ conduction band, and the Pr $4f$ level and core ($3d$ or $2p$) level, respectively. The electron creation operators for these states are denoted by $a_v^\dagger(k,\nu)$, $a_d^\dagger(k)$, $a_f^\dagger(\nu)$, and $a_c^\dagger$, respectively, with the use of the index k ($k=1-N$) of energy level in the valence and conduction bands, and the index ν ($\nu=1-14$) which specifies the spin and orbital degeneracies. The interactions U_{ff}, U_{fd}, U_{fc}, and U_{dc} denote, respectively, the Coulomb interactions between $4f$ electrons, between $4f$ and $5d$ electrons, between $4f$ electron and core hole, and between $5d$ electron and core hole.

The Hamiltonian H is diagonalized exactly with a finite value of N ($N=6$) and within the subspace including the $4f^1$, $4f^2$, and $4f^3$ configurations, both in the initial ($a_c^\dagger a_c=1$) and final ($a_c^\dagger a_c=0$) states of $3d$ XPS, $3d$ XAS, and L_3 XAS.

For instance, the ground state $|g\rangle$ (i.e., the initial state of these spectra) is obtained as a linear combination of basis states $|f^1\rangle$, $|f^2\rangle$, and $|f^3\rangle$, where

$$|f'\rangle=\frac{1}{\sqrt{N_f}}\sum_{\nu'}a_f^\dagger(\nu')\left[\prod_{k,\nu}a_v^\dagger(k,\nu)\right]a_c^\dagger|\,\text{vac}\,\rangle\ ,$$

and $|f^2\rangle$ and $|f^3\rangle$ are obtained from $|f^1\rangle$ by transferring one and two electrons from the valence band to the $4f$ states. For more details on the diagonalization of H, one can refer to the similar calculation for CeO_2 given by Jo and Kotani in Ref. 9.

When H is diagonalized, the spectra of $3d$ XPS, $3d$ XAS, and L_3 XAS are calculated in the following forms:

$$F_{3d\ \mathrm{XPS}}(E_B)=\sum_h|\langle h|a_c|g\rangle|^2L(E_B-E_h+E_g)\ ,$$

$$F_{3d\ \mathrm{XAS}}(\omega)=\sum_i|\langle i|a_f^\dagger(\nu)a_c|g\rangle|^2L(\omega-E_i+E_g)\ ,$$

$$F_{L_3\ \mathrm{XAS}}(\omega)=\frac{1}{N}\sum_j|\langle j|\sum_k a_d^\dagger(k)a_c|g\rangle|^2L(\omega-E_j+E_g)\ ,$$

where E_g is the ground-state energy, $|h\rangle$'s, $|i\rangle$'s, and $|j\rangle$'s are, respectively, the final states of $3d$ XPS, $3d$ XAS, and L_3 XAS, with the energies E_h's, E_i's, and E_j's, and $L(x)$ is defined by

$$L(x)=\Gamma/[\pi(x^2+\Gamma^2)]\ ,$$

where $x=\omega-E_j+E_g$ for XAS and $x=E_B-E_h+E_g$ for XPS. Here E_B is the binding energy, ω is the incident photon energy, and Γ represents the spectral broadening

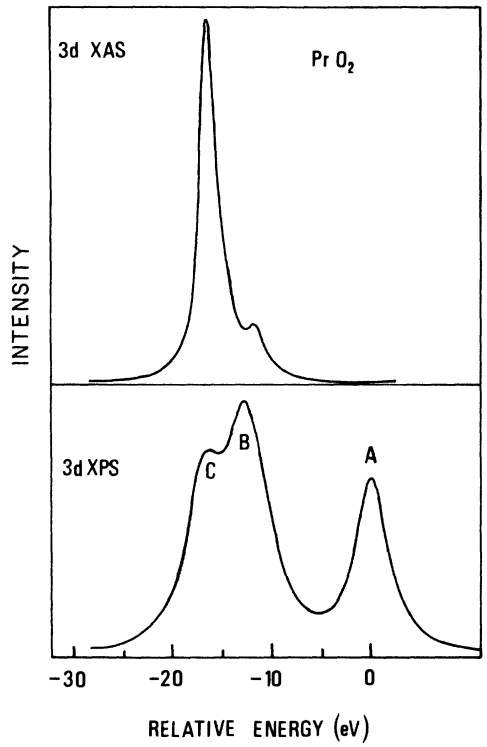

FIG. 4. Calculated $3d$ XAS (upper curve) and $3d$ XPS (lower curve) spectrum of PrO_2 using the many-body theory described in the text showing the many-body final state.

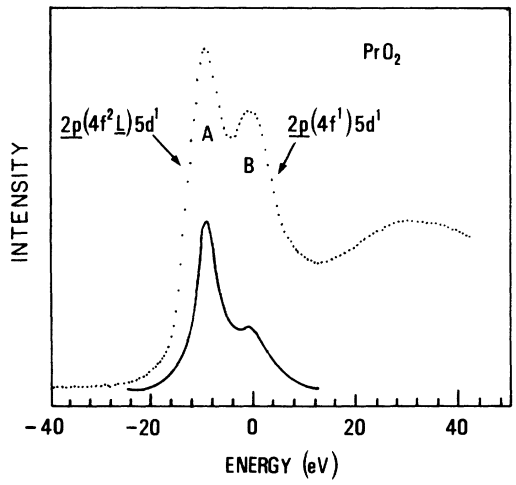

FIG. 5. Experimental L_3 XAS of PrO_2 (dotted curve) and theoretical many-body calculation of $2p\rightarrow 5d$ atomiclike transitions in the L_3 XAS spectrum (solid curve).

due to the lifetime of the core hole, as well as the multiplet effect and the experimental resolution.

In Fig. 4 we show the calculated result of $3d$ XPS and $3d$ XAS. We take the following parameter values: $\varepsilon_f^0-\varepsilon_v^0=-10$ eV, $U_{ff}=10.5$ eV, $U_{fc}=13$ eV, $V=0.45$ eV, and $\Gamma=2$ eV where ε_v^0 is the center of the valence band and its width W is taken to be 3 eV. These values are not very different from those used in the analysis for CeO_2 (Refs. 9–11) except that ε_f^0 is much lower and hybridization energy V is smaller than those of CeO_2. Since the energy separation (in the limit of vanishing V) ΔE between the $4f^1$ and $4f^2\underline{L}$ ionic configurations in the initial state is approximately given by $\Delta E=\varepsilon_f^0-\varepsilon_v^0+U_{ff}$, $\Delta E=0.5$ eV is found to be comparable with $V=0.45$ eV in the present analysis.

Therefore, the $4f^1$ and $4f^2\underline{L}$ configurations are mixed strongly through V, giving the ground state and we obtain the average $4f$ electron number $n_f=1.6$ in the ground state $\Psi_g=a\,|\,4f^1\rangle+b\,|\,4f^2\underline{L}\,\rangle$. This value is in good agreement with the value of $n_f=1.58$ predicted by the energy-band calculation by Koelling *et al.*[3] and also with the value $n_f=1.56$ estimated from the L_3 XAS data.[11]

By this analysis it is found that the three peaks of the $3d$ XPS come mainly from the $4f^1$, $4f^2\underline{L}$ and $4f^3\underline{L}$ configurations in the final state, in the order of decreasing binding energy. The $4f^2\underline{L}$ and $4f^3\underline{L}$ final states are mixed together considerably through V. The energy separations of the three peaks are in very good agreement with the experimental result, and the agreement of their relative intensities with experimental ones is also fairly good, although the intensity of the highest binding-energy peak seems to be somewhat larger than the experimental result.

Finally, we show in Fig. 5 the result of L_3 XAS. By using the values of $U_{fd}=5$ eV and $U_{dc}=7$ eV, we obtain the two-peak structure of L_3 XAS with the higher-intensity peak in the lower-energy side, in agreement with experiment. (With smaller values of U_{fd} and/or U_{dc}, we have three-peak structure or two-peak and one shoulder structure which does not agree with experiment.)

The role of $-U_{dc}$ is to localize the excited $5d$ electron near the core hole, and then by the effect of U_{fd} the energies of the $4f^2\underline{L}5,\varepsilon d^1$ and $4f^3\underline{L}^2 5,\varepsilon d^1$ final states are elevated by U_{fd} and $2U_{fd}$ with respect to that of the $4f^1 5,\varepsilon d^1$ state. As a result, the mixing between $4f^2\underline{L}5,\varepsilon d^1$ and $4f^3\underline{L}^2 5,\varepsilon d^1$ states decreases, and the L_3 XAS exhibits two peaks mainly corresponding to the $[4f^1]$ (higher-energy peak) and $[4f^2\underline{L}]$ (lower-energy one) configurations with a small contribution of $4f^3\underline{L}^2$ configuration overlapped with the $4f^1$ peak. The situation is similar to the L_3 XAS of CeO_2, where the two peaks correspond mainly to the $4f^0$ and $4f^1\underline{L}$ configurations.

More details of the theoretical analysis, including the calculation of the valence-band photoemission, resonant photoemission, and bremsstrahlung isochromat spectroscopy, will be published elsewhere.

CONCLUSIONS

The core-level spectra of PrO_2 clearly indicate the need for a many-body description of its ground state. Evidence for mixing of $4f^1$ and $4f^2\underline{L}$ configurations in the ground state is obtained by $3d$ XPS, $2p$ XAS, and $3d$ XAS where the final states are quite different because the effective perturbation energies on the localized $4f$ electrons are $|\,U_{fc}\,|$, $|\,U_{fc}-U_{fd}\,|$, and $|\,U_{fc}-U_{ff}\,|$, respectively. Therefore the relaxation of the $4f$ orbital is strongly reduced going from $3d$ XPS to $3d$ XAS but evidence of mixing of the two many-body configurations in each spectroscopy has been found.

In conclusion PrO_2 has been found to be a highly correlated and covalent oxide, like CeO_2, for which a many-body description of the core-level spectroscopies is required.

[1] P. Burroughs, A. Hamnett, A. F. Orchard, and G. Thornton, J. Chem. Soc. Dalton Trans. **17**, 1686 (1976).

[2] G. Thornton and M. J. Dempsey, Chem. Phys. Lett. **77**, 409 (1981).

[3] D. D. Koelling, A. M. Boering, and J. H. Wood, Solid State Commun. **47**, 227 (1983).

[4] A. Fujimori, Phys. Rev. B **28**, 2281 (1983); **28**, 4489 (1983); Phys. Rev. Lett. **53**, 2581 (1984).

[5] E. Wuilloud, B. Delley, W. D. Schneider, and Y. Baer, Phys. Rev. Lett. **53**, 202 (1984); **53**, 2519 (1984).

[6] W. D. Schneider, B. Delley, E. Wuilloud, J. M. Imer, and Y. Baer, Phys. Rev. B **32**, 6819 (1985).

[7] A. Kotani, H. Mizuta, T. Jo, and J. C. Parlebas, Solid State Commun. **53**, 805 (1985).

[8] A. Kotani and J. C. Parlebas, J. Phys. (Paris) **46**, 77 (1985).

[9] T. Jo and A. Kotani, J. Phys. Soc. Jpn. **55**, 2457 (1986).

[10] A. Bianconi, A. Marcelli, M. Tomellini, and I. Davoli, J. Magn. Magn. Mater. **47-48**, 209 (1985).

[11] A. Bianconi, A. Marcelli, H. Dexpert, R. Karnatak, A. Kotani, T. Jo, and J. Petiau, Phys. Rev. B **35**, 806 (1987).

[12] A. Bianconi, I. Davoli, S. Della Longa, J. Garcia, K. B. Garg, A. Kotani, and A. Marcelli, in *Theoretical and Experimental Aspects of Valence Fluctuations and Heavy Fermions,* edited by L. C. Gupta and S. K. Malik (Plenum, New York, 1987), pp. 243–251.

[13] G. Kaindl, G. K. Wertheim, G. Schmiester, and E. V. Sampathkumaran, Phys. Rev. Lett. **58**, 606 (1987).

[14] F. Marabelli and P. Wachter, Phys. Rev. B **36**, 1238 (1987).

[15] R. C. Karnatak, J. M. Esteva, H. Dexpert, M. Gasnier, P. E. Caro, and L. Albert, Phys. Rev. B **36**, 1745 (1987).

[16] M. McKelvy and LeRoy Eyring, J. Cryst. Growth **62**, 635 (1983).

[17] O. Gunnarsson and K. Schonhammer, Phys. Rev. B **28**, 4315 (1983).

[18] N. E. Bickers, D. L. Cox, and J. W. Wilkins, Phys. Rev. Lett. **54**, 230 (1985).

[19] J. W. Allen and R. M. Martin, Phys. Rev. Lett. **49**, 1106 (1982).

[20] J. W. Allen, S. J. Oh, M. B. Maple, and M. S. Torikachvili, Phys. Rev. B **28**, 5347 (1983).

[21] J. W. Allen, S. J. Oh, O. Gunnarsson, K. Schonhammer, M. B. Maple, and M. S. Torikachvili, Adv. Phys. **35**, 275 (1986).